Heliyon 9 (2023) e17445

Contents lists available at ScienceDirect

Heliyon

journal homepage: www.cell.com/heliyon

Research article

Micromechanical analysis for effective thermal and electromagnetic properties of composite materials containing anisotropical and ellipsoidal fillers oriented randomly

Hiroyuki Ono

Division of Mechanical Engineering, Kyoto Institute of Technology, 1 Matsugasaki, Sakyo-ku, Kyoto City, Kyoto, Japan

A R T I C L E I N F O

Keywords:
Thermal and electromagnetic properties
Ellipsoidal filler
Anisotropy
Micromechanics
Self-consistent method
Mori-Tanaka's theory

A B S T R A C T

In this study, micromechanical modeling will be performed for composite materials containing fillers oriented randomly in the matrix. The purpose of this study is to derive more general and explicit solutions for the effective thermal and electromagnetic properties of such composite materials without restricting the properties and shapes of the fillers. For this purpose, it is assumed that the physical properties of the filler are the same anisotropic properties as orthorhombic materials, and the shape of the fillers is ellipsoidal. This model is analyzed by micromechanics combining the Eshelby's equivalent inclusion method with the self-consistent method or the Mori-Tanaka's theory. Solutions of the effective thermal and electromagnetic properties both for composite materials containing many kinds of fillers with different shapes and physical properties and for polycrystalline materials can be also derived. Using the obtained solutions, the effect of the shape, the anisotropy, and the volume fraction of the filler on the effective thermal conductivity is examined for the carbon filler / polyethylene and the two types of quartz particles (and voids) / polyethylene. As a result, for the carbon filler / polyethylene, it is found that the effective thermal conductivity of the material when the shape of the filler is flat is about 20% higher than that when the shape of the filler is fibrous. Furthermore, when the shape of the carbon filler is flat, the result when the carbon filler is assumed to be isotropic is significantly different from that when the filler is assumed to be anisotropic. From the above, when the filler is oriented randomly in the material, it is found that simultaneously considering not only the shape of the filler but also its anisotropic properties is important to accurately evaluate the effective physical properties of the composite material. For two types of quartz particles (and voids) / polyethylene materials, the experimental result agrees better with the result of the Mori-Tanaka's theory than that of the self-consistent method, even if the volume fraction of the filler is more than 50%. From the above results, it is found that the analytical solutions of this study can generally explain the experimental results and can be applied to actual materials.

1. Introduction

Most of the practical composite materials in which fillers are dispersed in the matrix are produced by pressing and heating SMC (sheet molding compound) or BMC (bulk molding compound) placed in a mold. Short fibers, particles, and flakes are used as fillers of

E-mail address: ono@mech.kit.ac.jp.

https://doi.org/10.1016/j.heliyon.2023.e17445
Received 21 February 2023; Received in revised form 16 June 2023; Accepted 16 June 2023

Available online 22 June 2023

SMC or BMC. This molding method is already widely used in industrial products. In recent years, the movement to apply 3D printing technology to the fabrication of parts made from composite materials is progressive, since there is little material loss and parts with complicated shapes can be manufactured. For example, fused deposition modeling (FDM) as one of the 3D printing technology can produce a part made from a composite material by stacking resin filaments containing metal or ceramic fillers. By using this molding technology, it is possible to create parts with optimal values of mechanical, thermal, and electromagnetic properties [1]. In these composite materials, from the view point of material design, the properties of the entire material should be homogeneous and isotropic. Therefore, composite materials are manufactured in such a way that the fillers are oriented randomly and dispersed uniformly in the resin matrix. The development of analytical tools that can accurately and quickly obtain the effective physical properties of composite materials containing such randomly oriented fillers will play increasingly an important role in the future.

There are many analytical studies on the thermal and electromagnetic properties of two-phase composites composed of fillers and a matrix [2]. For these material properties, approaches based on homogenization theory and numerical analysis such as the finite element method are available. Some analyses use the finite element method for effective thermal conductivity and dielectric constants of the materials containing spherical fillers or fibrous ones [3] [4]. However, such numerical approaches require a huge number of element divisions to represent the three-dimensional structure of materials, and it takes a long time to calculate these effective physical properties of the materials. In addition, it has the disadvantage that the influence of the shape of the filler on the effective physical properties of a material cannot be easily handled. Therefore, homogenization theory may be an available analytical method for the design of practical materials. As homogenization theories used widely, there are the variational principle, the Mori-Tanaka's theory [5], the self-consistent method [6], the differential scheme [7] and so on. Using the variational principle, Hashin et al. derived solutions for the upper and lower bounds of the effective magnetic permeability for multiphase composite materials in which fillers are randomly oriented in the matrix [8]. Benvaniste derived the effective thermal conductivity of a particulate composite, by using the generalized self-consistent method and the Mori-Tanaka theory [9]. As the analysis using the Mori-Tanaka's theory, Hatta et al. derived the solution of the effective thermal conductivity of composite materials when the filler is isotropic and its shape is spheroidal [10]. In this analysis, Hatta et al. applied the Eshelby's equivalent inclusion method to problems of heat conduction and derived the Eshelby's tensor for these problems [11] [12]. Regarding the analysis using the self-consistent method, Kanaun et al. derived the solution of the effective thermal and electromagnetic properties when the physical property of the filler is isotropic and its shape is spherical [13]. However, these analyzes are limited to cases where the physical properties of fillers are isotropic and their shapes are spheroidal or spherical.

Regarding the shape of the filler, experimental results have been reported that the thermal conductivity of the composite material varies significantly due to the subtle differences in the shape of the filler [14] [15] [16]. Regarding the anisotropy of fillers, there are some fillers whose properties are anisotropic, depending on their structure resulting from the manufacturing method of fillers. Carbon fibers are the typical example [17] [18]. Therefore, it is desirable to derive an analytical solution of the effective properties of composite materials that can handle simultaneously arbitrary shapes and anisotropy of fillers.

From the above, the purpose of this study is to obtain more general solutions to the effective thermal and electromagnetic properties of composite materials containing filler oriented randomly in the material. In this analysis, without loss of generality, it is assumed that the physical properties of the filler are the same anisotropic properties as orthorhombic materials, and the shape of fillers is arbitrary ellipsoidal. This model is analyzed by micromechanics combining the Eshelby's equivalent inclusion method with the self-consistent method or the Mori-Tanaka's theory. In addition, the analysis of effective thermal and electromagnetic properties for composite materials containing many kinds of fillers whose properties and shapes are different from each other and for polycrystalline materials will be also performed. Furthermore, by using solutions obtained in this analysis, it is performed to calculate the effect of the shape, the anisotropy, and the volume fraction of fillers on the effective thermal conductivity, and to examine the usefulness of derived solutions by comparing these analytical results with experimental ones.

2. Analysis of effective thermal and electromagnetic properties of composite materials containing ellipsoidal fillers oriented randomly

In this chapter, effective thermal conductivity, permittivity (dielectric constant), electrical conductivity, and magnetic permeability of composite materials containing ellipsoidal fillers oriented randomly are examined. The ranks of tensors related to fields and physical properties in these problems are all the same, that is, the tensor of fields is first-order and that of property is second-order. Moreover, the constitutive equation and equilibrium one are expressed in the same form. Thus, by this analogy, if one of these physical properties can be solved, all other properties can be automatically found by a simple substitution of symbols [19]. Here, we take the dielectric problem as an example.

2.1. Analysis by the self-consistent method

2.1.1. Analytical model

Fig. 1 shows a composite material containing randomly oriented ellipsoidal fillers in the matrix, and the fillers are shown as the shaded area. Fillers are classified according to their orientation, and regions of fillers and the entire material are denoted by $\Omega(i)$ and D respectively. A global coordinate system ${}^{G}x_i$ is taken along the direction of the dielectric flux D_i^0 acting externally on the material, and a local coordinate system ${}^{L(i)}x_i$ is taken along the direction of the principal semi-axis of a filler $\Omega(i)$ as shown in Fig. 1. From now on, we will add ^{G} or ${}^{L(i)}$ to the left shoulder of the symbols for field quantities to indicate that they are quantities related to the global coordinate system or the local coordinate one. All fillers have the same ellipsoidal shape, and the axial length of fillers in the

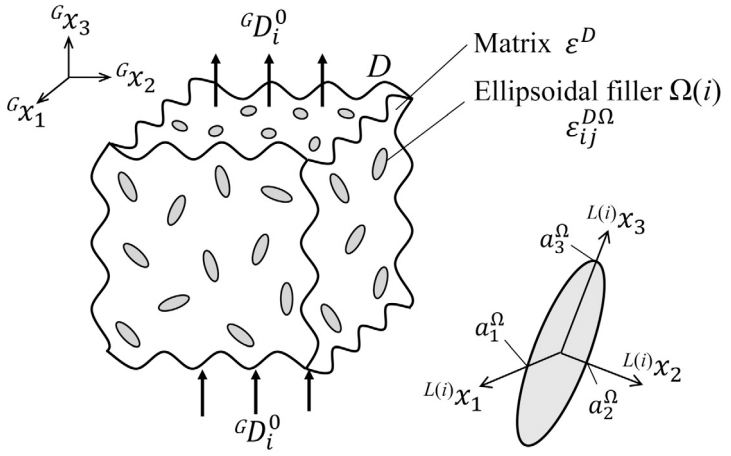

Fig. 1. Composite material containing many ellipsoidal fillers oriented randomly.

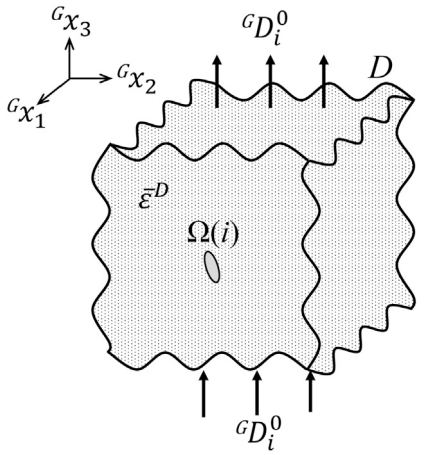

Fig. 2. Model smeared out with unknown effective dielectric constant in the global coordinate system.

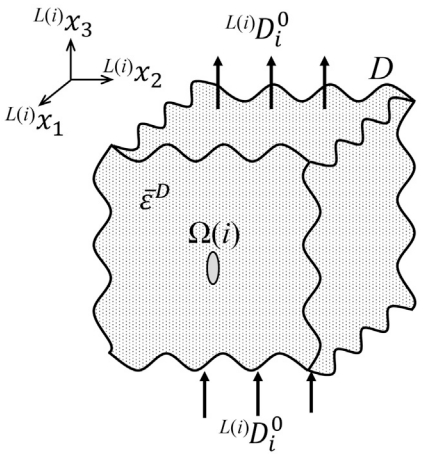

Fig. 3. Model smeared out with unknown effective dielectric constant in the local coordinate system.

direction of ${}^{L(i)}x_i$ is denoted by a_i^Ω. In addition, all fillers have the same permittivity as an orthorhombic material, as shown in the following equation

$$\boldsymbol{\varepsilon}^{D\Omega} = \begin{bmatrix} \varepsilon_{11}^{D\Omega} & 0 & 0 \\ 0 & \varepsilon_{22}^{D\Omega} & 0 \\ 0 & 0 & \varepsilon_{33}^{D\Omega} \end{bmatrix}. \tag{1}$$

The permittivity of the matrix is denoted by ε^D and it's isotropic. In addition, the eigen electric field $E_i^{p\Omega}$ is given in the region of filler $\Omega(i)$, and its magnitude is assumed to be the same for all fillers. This electric field corresponds to the residual strain in the elastic problem, but we do not mention what the source of this is. $f_{(i)}$ is the volume fraction of filler $\Omega(i)$ in the material, and f is the total volume fraction of fillers. That is, $f = \sum_{i=1}^{n} f_{(i)}$.

Fig. 2 shows the model in which the material surrounding a filler $\Omega(i)$ shown in Fig. 1 is replaced by a material with unknown effective permittivity $\bar{\varepsilon}^D$. Note that the property of the entire material is macroscopically isotropic because the fillers are randomly oriented in the material. Furthermore, the external dielectric flux ${}^{G}D_i^0$ in Fig. 2 is transformed into ${}^{L(i)}D_i^0$ that is the quantity in the local coordinate system ${}^{L(i)}x_i$ taken along the direction of the principal semi-axis of the filler $\Omega(i)$. This model is shown in Fig. 3. Analysis of the model in Fig. 2 requires coordinate transformation for the Eshelby tensor that appears in the equivalent equation shown later, and cannot derive smartly the solutions of the equivalent equation. Therefore, in this analysis, the model in Fig. 3 will be used as the analytical model.

2.1.2. Analysis of effective permittivity

The equivalent equation for the filler $\Omega(i)$ shown in Fig. 3 is given by

$${}^{L(i)}D_i^0 + {}^{L(i)}D_i^\infty = \varepsilon_{ij}^{D\Omega}\left\{{}^{L(i)}\overline{E}_j + (S_{jk}^\Omega - I_{jk})\,{}^{L(i)}E_k^{**\Omega(i)} + {}^{L(i)}E_j^{*\Omega(i)}\right\}$$

$$= \delta_{ij}\,\overline{\varepsilon}^{D}\left\{{}^{L(i)}\overline{E}_j + (S^{\Omega}_{jk} - I_{jk})\,{}^{L(i)}E^{**\Omega(i)}_{k}\right\}, \tag{2}$$

where ${}^{L(i)}D^{\infty}_{i}$ is the eigen dielectric flux in the region $\Omega(i)$, ${}^{L(i)}E^{**\Omega(i)}_{i}$ is the sum of the eigen electric field $E^{p\Omega}_{i}$ and the unknown equivalent eigen electric field ${}^{L(i)}E^{*\Omega(i)}_{i}$ that substitutes for the difference in permittivity between the filler and the matrix. That is, ${}^{L(i)}E^{**\Omega(i)}_{i}$ is expressed as

$${}^{L(i)}E^{**\Omega(i)}_{i} = E^{p\Omega}_{i} + {}^{L(i)}E^{*\Omega(i)}_{i}\,. \tag{3}$$

Since the eigen electric field $E^{p\Omega}_{i}$ is usually considered to be a quantity given along the direction of the principal semi-axis of $\Omega(i)$, the left shoulder of $E^{p\Omega}_{i}$ is not attached with ${}^{L(i)}$ representing the local coordinate system. The unknown quantity to be derived is the equivalent eigen electric field ${}^{L(i)}E^{*\Omega(i)}_{i}$, but to simplify the derivation of Eq. (2), ${}^{L(i)}E^{**\Omega(i)}_{i}$ in Eq. (3), that is sum of $E^{p\Omega}_{i}$ and ${}^{L(i)}E^{*\Omega(i)}_{i}$, will be obtained as the unknown quantity.

S^{Ω}_{ij} is the Eshelby tensor of region Ω and given by

$$\mathbf{S}^{\Omega} = \begin{bmatrix} S^{\Omega}_{11} & 0 & 0 \\ 0 & S^{\Omega}_{22} & 0 \\ 0 & 0 & S^{\Omega}_{33} \end{bmatrix} = \begin{bmatrix} H^{\Omega}_{1} & 0 & 0 \\ 0 & H^{\Omega}_{2} & 0 \\ 0 & 0 & H^{\Omega}_{3} \end{bmatrix}. \tag{4}$$

H^{Ω}_{i} is called the geometrical factor and the relation $H^{\Omega}_{1} + H^{\Omega}_{2} + H^{\Omega}_{3} = 1$ holds [20]. Geometrical factors for various shapes of filler are given in Appendix A. I_{ij} is the identity matrix, and ${}^{L(i)}\overline{E}_i$ is the electric field occurred over the material by ${}^{L(i)}D^{0}_{i}$. Substituting Eqs. (1) and (4) into Eq. (2), and solving for the equivalent eigen electric field, we obtain

$${}^{L(i)}E^{**\Omega(i)}_{1} = -A^{\Omega}_{1}({}^{L(i)}\overline{E}_1 - L^{\Omega}_{1}E^{p\Omega}_{1})\,, \tag{5}$$

where

$$L^{\Omega}_{1} = \frac{\varepsilon^{D\Omega}_{11}}{\varepsilon^{D\Omega}_{11} - \overline{\varepsilon}^{D}} \quad , \qquad A^{\Omega}_{1} = \frac{1}{L^{\Omega}_{1} + H^{\Omega}_{1} - 1}\,. \tag{6}$$

Components 2 and 3 can be found by substituting 2 or 3 for subscript 1 in Eqs. (5) and (6). The total electric field ${}^{L(i)}E^{total}_{i}$ in region $\Omega(i)$ in the local coordinate system is given from Eqs. (2), (4) and (5) as follows:

$$\begin{aligned} &{}^{L(i)}E^{total}_{i} = {}^{L(i)}\overline{E}_i + S^{\Omega}_{ij}\,{}^{L(i)}E^{**\Omega(i)}_{j}\,. \\ &\therefore {}^{L(i)}E^{total}_{1} = (1 - H^{\Omega}_{1}A^{\Omega}_{1})\,{}^{L(i)}\overline{E}_1 + L^{\Omega}_{1}H^{\Omega}_{1}A^{\Omega}_{1}E^{p\Omega}_{1}\,. \end{aligned} \tag{7a}$$

The total dielectric flux ${}^{L(i)}D^{total}_{i}$ in the region $\Omega(i)$ in the local coordinate system is obtained from Eqs. (1), (2) and (7a) as follows:

$$\begin{aligned} &{}^{L(i)}D^{total}_{i} = {}^{L(i)}D^{0}_{i} + {}^{L(i)}D^{\infty}_{i} = \varepsilon^{D\Omega}_{ij}({}^{L(i)}E^{total}_{j} - E^{p\Omega}_{j})\,. \\ &\therefore {}^{L(i)}D^{total}_{1} = \varepsilon^{D\Omega}_{11}\left\{(1 - H^{\Omega}_{1}A^{\Omega}_{1})\,{}^{L(i)}\overline{E}_1 - (1 - L^{\Omega}_{1}H^{\Omega}_{1}A^{\Omega}_{1})E^{p\Omega}_{1}\right\}. \end{aligned} \tag{8a}$$

Representing Eqs. (7a) and (8a) as matrix form,

$${}^{L(i)}\mathbf{E}^{total} = \mathbf{P}^{\Omega}\,{}^{L(i)}\overline{\mathbf{E}} - \mathbf{P}^{p\Omega}\mathbf{E}^{p\Omega}\,, \tag{7b}$$

$${}^{L(i)}\mathbf{D}^{total} = \boldsymbol{\varepsilon}^{D\Omega}({}^{L(i)}\mathbf{E}^{total} - \mathbf{E}^{p\Omega}) = \boldsymbol{\varepsilon}^{D\Omega}\left\{\mathbf{P}^{\Omega}\,{}^{L(i)}\overline{\mathbf{E}} - (\mathbf{P}^{p\Omega} - \mathbf{I})\mathbf{E}^{p\Omega}\right\}, \tag{8b}$$

where $\mathbf{I}$ is the identity matrix, and $\mathbf{P}^{\Omega}$ and $\mathbf{P}^{p\Omega}$ are given by

$$\mathbf{P}^{\Omega} = \begin{bmatrix} P^{\Omega}_{11} & 0 & 0 \\ 0 & P^{\Omega}_{22} & 0 \\ 0 & 0 & P^{\Omega}_{33} \end{bmatrix} \quad , \qquad \mathbf{P}^{p\Omega} = \begin{bmatrix} P^{p\Omega}_{11} & 0 & 0 \\ 0 & P^{p\Omega}_{22} & 0 \\ 0 & 0 & P^{p\Omega}_{33} \end{bmatrix} \quad , \tag{9a}$$

$$P^{\Omega}_{11} = 1 - H^{\Omega}_{1}A^{\Omega}_{1} = \frac{\overline{\varepsilon}^{D}}{H^{\Omega}_{1}\varepsilon^{D\Omega}_{11} + (1 - H^{\Omega}_{1})\overline{\varepsilon}^{D}} \quad , \qquad P^{p\Omega}_{11} = -L^{\Omega}_{1}H^{\Omega}_{1}A^{\Omega}_{1} = -\frac{H^{\Omega}_{1}\varepsilon^{D\Omega}_{11}}{H^{\Omega}_{1}\varepsilon^{D\Omega}_{11} + (1 - H^{\Omega}_{1})\overline{\varepsilon}^{D}}\,. \tag{9b}$$

Next, we consider equations of coordinate transformation for the electric field and dielectric flux from the global coordinate system to the local coordinate one, or vice versa. Let ${}^{L}\mathbf{E}$ and ${}^{L}\mathbf{D}$ denote the electric field and the dielectric flux in the local coordinate system, and ${}^{G}\mathbf{E}$ and ${}^{G}\mathbf{D}$ denote them in the global coordinate system. Then, equations of coordinate transformation are expressed by

$${}^{L}\mathbf{E} = \boldsymbol{l}\,{}^{G}\mathbf{E} \quad , \qquad {}^{L}\mathbf{D} = \boldsymbol{l}\,{}^{G}\mathbf{D}\,, \tag{10a}$$

$${}^{G}\mathbf{E} = \boldsymbol{l}^{t}\,{}^{L}\mathbf{E} = \boldsymbol{l}^{-1}\,{}^{L}\mathbf{E} \quad , \qquad {}^{G}\mathbf{D} = \boldsymbol{l}^{t}\,{}^{L}\mathbf{D} = \boldsymbol{l}^{-1}\,{}^{L}\mathbf{D}\,, \tag{10b}$$

where $\boldsymbol{l}$ is the matrix of coordinate transformation and ^{t} represents the transpose of matrix. Fig. 4 shows the spherical coordinate system expressed in Euler angles, where θ, ϕ, and ψ are the zenith, azimuth, and rotation angles of a filler. In the case of the y-

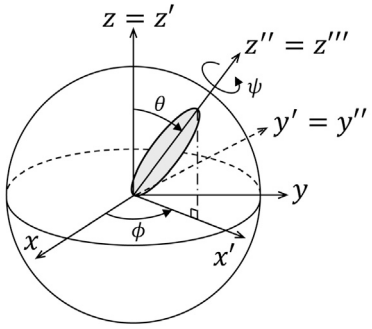

Fig. 4. Spherical coordinate system expressed by Euler angles.

convention, the coordinate transformation is performed by first rotating an azimuth angle ϕ around the z-axis, then a zenith angle θ around the y-axis, and finally a rotation angle ψ around the z-axis again. The matrix of coordinate transformation in the y-convention $\boldsymbol{l}$ is given as follows [21]:

$$\begin{aligned}\boldsymbol{l} &= \begin{bmatrix} l_{11} & l_{12} & l_{13} \\ l_{21} & l_{22} & l_{23} \\ l_{31} & l_{32} & l_{33} \end{bmatrix} = \begin{bmatrix} \cos\psi & \sin\psi & 0 \\ -\sin\psi & \cos\psi & 0 \\ 0 & 0 & 1 \end{bmatrix} \begin{bmatrix} \cos\theta & 0 & -\sin\theta \\ 0 & 1 & 0 \\ \sin\theta & 0 & \cos\theta \end{bmatrix} \begin{bmatrix} \cos\phi & \sin\phi & 0 \\ -\sin\phi & \cos\phi & 0 \\ 0 & 0 & 1 \end{bmatrix} \\ &= \begin{bmatrix} \cos\theta\cos\phi\cos\psi - \sin\phi\sin\psi & \cos\theta\sin\phi\cos\psi + \cos\phi\sin\psi & -\sin\theta\cos\psi \\ -\cos\theta\cos\phi\sin\psi - \sin\phi\cos\psi & -\cos\theta\sin\phi\sin\psi + \cos\phi\cos\psi & \sin\theta\sin\psi \\ \sin\theta\cos\phi & \sin\theta\sin\phi & \cos\theta \end{bmatrix}. \end{aligned} \tag{11}$$

Using the relation of Eq. (10), the transformation for the total electric field ${}^{L(i)}\mathbf{E}^{total}$ and the total dielectric flux ${}^{L(i)}\mathbf{D}^{total}$ in Eqs. (7b) and (8b) to the global coordinate system are expressed as

$${}^{G}\mathbf{E}^{total} = \{\boldsymbol{l}^{(i)}\}^{-1}\ \mathbf{P}^{\Omega}\ \boldsymbol{l}^{(i)}\ {}^{G}\overline{\mathbf{E}} - \{\boldsymbol{l}^{(i)}\}^{-1}\ \mathbf{P}^{p\Omega}\mathbf{E}^{p\Omega}\ , \tag{7c}$$

$${}^{G}\mathbf{D}^{total} = \{\boldsymbol{l}^{(i)}\}^{-1}\ \boldsymbol{\varepsilon}^{D\Omega}\ \mathbf{P}^{\Omega}\ \boldsymbol{l}^{(i)}\ {}^{G}\overline{\mathbf{E}} - \{\boldsymbol{l}^{(i)}\}^{-1}\ \boldsymbol{\varepsilon}^{D\Omega}\ (\mathbf{P}^{p\Omega} - \mathbf{I})\mathbf{E}^{p\Omega}\ . \tag{8c}$$

From Eqs. (7c), (8c), and (11), taking the summation of the total electric field and the total dielectric flux of all fillers and the matrix yields the macroscopic total electric field ${}^{G}\overline{\mathbf{E}}$ and the macroscopic total dielectric flux ${}^{G}\overline{\mathbf{D}}$ as follows:

$$\begin{aligned}{}^{G}\overline{\mathbf{E}} &= \sum_{i=1}^{n} f_{(i)}\ {}^{G}\mathbf{E}^{total} + \left(1 - \sum_{i=1}^{n} f_{(i)}\right) {}^{G}\mathbf{E}^{m} \\ &= \frac{1}{8\pi^2} f \int_0^{\pi}\int_0^{2\pi}\int_0^{2\pi} sin\theta \left(\boldsymbol{l}^{-1}\ \mathbf{P}^{\Omega}\ \boldsymbol{l}\ {}^{G}\overline{\mathbf{E}} - \boldsymbol{l}^{-1}\ \mathbf{P}^{p\Omega}\mathbf{E}^{p\Omega}\right) d\theta\, d\phi\, d\psi + (1-f)\ {}^{G}\mathbf{E}^{m} \\ &= \frac{1}{3} f (P_{11}^{\Omega} + P_{22}^{\Omega} + P_{33}^{\Omega}) {}^{G}\overline{\mathbf{E}} + (1-f)\ {}^{G}\mathbf{E}^{m}\ , \end{aligned} \tag{12}$$

$$\begin{aligned}{}^{G}\overline{\mathbf{D}} &= \sum_{i=1}^{n} f_{(i)}\ {}^{G}\mathbf{D}^{total} + \left(1 - \sum_{i=1}^{n} f_{(i)}\right) {}^{G}\mathbf{D}^{m} \\ &= \frac{1}{8\pi^2} f \int_0^{\pi}\int_0^{2\pi}\int_0^{2\pi} sin\theta \left(\boldsymbol{l}^{-1}\boldsymbol{\varepsilon}^{D\Omega}\ \mathbf{P}^{\Omega}\ \boldsymbol{l}\ {}^{G}\overline{\mathbf{E}} - \boldsymbol{l}^{-1}\boldsymbol{\varepsilon}^{D\Omega}\ (\mathbf{P}^{p\Omega} - \mathbf{I})\mathbf{E}^{p\Omega}\right) d\theta\, d\phi\, d\psi + (1-f) {}^{G}\mathbf{D}^{m} \\ &= \frac{1}{3} f (\varepsilon_{11}^{D\Omega}\ P_{11}^{\Omega} + \varepsilon_{22}^{D\Omega}\ P_{22}^{\Omega} + \varepsilon_{33}^{D\Omega}\ P_{33}^{\Omega}) {}^{G}\overline{\mathbf{E}} + (1-f) {}^{G}\mathbf{D}^{m}\ . \end{aligned} \tag{13}$$

Note that from Eqs. (12) and (13) the integral concerning the eigen electric field $\mathbf{E}^{p\Omega}$ vanishes as a result. ${}^{G}\mathbf{E}^{m}$ and ${}^{G}\mathbf{D}^{m}$ in these equations are the total electric field and the total dielectric flux of the matrix respectively, and the following relation between them holds.

$${}^{G}D_i^m = \delta_{ij}\varepsilon^{D}\ {}^{G}E_j^m \quad or \quad {}^{G}\mathbf{D}^m = \varepsilon^{D}\ {}^{G}\mathbf{E}^m\ . \tag{14}$$

About Eqs. (12) and (13), if ${}^{G}\mathbf{E}^{m}$ and ${}^{G}\mathbf{D}^{m}$ are eliminated using the relation of Eq. (14), then the relation between ${}^{G}\overline{\mathbf{E}}$ and ${}^{G}\overline{\mathbf{D}}$ can be obtained as follows:

$${}^{G}\overline{\mathbf{D}} = \left[\varepsilon^{D} + \frac{1}{3} f \left\{ P_{11}^{\Omega}(\varepsilon_{11}^{D\Omega} - \varepsilon^{D}) + P_{22}^{\Omega}(\varepsilon_{22}^{D\Omega} - \varepsilon^{D}) + P_{33}^{\Omega}(\varepsilon_{33}^{D\Omega} - \varepsilon^{D}) \right\}\right] {}^{G}\overline{\mathbf{E}}\ . \tag{15}$$

On the other hand, ${}^{G}\overline{\mathbf{E}}$ and ${}^{G}\overline{\mathbf{D}}$ have the following relation through the effective permittivity $\overline{\varepsilon}^{D}$ of the material.

$$ {}^{G}\overline{\mathbf{D}} = \overline{\varepsilon}^{D}\, {}^{G}\overline{\mathbf{E}} \,. \tag{16} $$

By equating Eq. (15) with Eq. (16) and using Eq. (9), the effective permittivity $\overline{\varepsilon}^{D}$ is finally obtained as

$$ \overline{\varepsilon}^{D} = \varepsilon^{D} + \frac{1}{3} f\, \overline{\varepsilon}^{D} \left\{ \frac{\varepsilon_{11}^{D\Omega} - \varepsilon^{D}}{H_1^{\Omega}\varepsilon_{11}^{D\Omega} + (1 - H_1^{\Omega})\overline{\varepsilon}^{D}} + \frac{\varepsilon_{22}^{D\Omega} - \varepsilon^{D}}{H_2^{\Omega}\varepsilon_{22}^{D\Omega} + (1 - H_2^{\Omega})\overline{\varepsilon}^{D}} + \frac{\varepsilon_{33}^{D\Omega} - \varepsilon^{D}}{H_3^{\Omega}\varepsilon_{33}^{D\Omega} + (1 - H_3^{\Omega})\overline{\varepsilon}^{D}} \right\} . \tag{17} $$

Note that Eq. (17) is an equation for the unknown $\overline{\varepsilon}^{D}$, so it is necessary to find the value of $\overline{\varepsilon}^{D}$ by numerical calculation.

2.2. Analysis by the Mori-Tanaka's theory

In this section, we perform the analysis using the concept of the Mori-Tanaka's theory. In this theory, the surrounding of a filler $\Omega(i)$ in the composite material shown in Fig. 1 is smeared out by unknown interaction dielectric flux $\tilde{D}_i$. This point is different from the self-consistent method. Therefore, in the models in Figs. 3 and 4, the unknown permittivity $\overline{\varepsilon}^{D}$ in the shaded area is replaced by the known permittivity ε^{D} of the matrix, and the unknown interaction dielectric flux $\tilde{D}_i$ acts on the entire material. Let E_i^0 and $\tilde{E}_i$ denote the external electric field and the interaction one corresponding to D_i^0 and $\tilde{D}_i$, respectively. Referring to Eq. (2), the equivalent equation for the filler $\Omega(i)$ is given by

$$ \begin{aligned} {}^{L(i)}D_i^0 + {}^{L(i)}\tilde{D}_i + {}^{L(i)}D_i^{\infty} &= \varepsilon_{ij}^{D\Omega}\left\{ {}^{L(i)}E_j^0 + {}^{L(i)}\tilde{E}_j + (S_{jk}^{\Omega} - I_{jk})\, {}^{L(i)}E_k^{**\Omega(i)} + {}^{L(i)}E_j^{*\Omega(i)} \right\} \\ &= \delta_{ij}\, \varepsilon^{D}\left\{ {}^{L(i)}E_j^0 + {}^{L(i)}\tilde{E}_j + (S_{jk}^{\Omega} - I_{jk})\, {}^{L(i)}E_k^{**\Omega(i)} \right\} . \end{aligned} \tag{18} $$

Relations between D_i^0 and E_i^0, $\tilde{D}_i$ and $\tilde{E}_i$ are as follows:

$$ D_i^0 = \delta_{ij}\varepsilon^{D} E_j^0 \quad , \quad \tilde{D}_i = \delta_{ij}\varepsilon^{D}\tilde{E}_j \,. \tag{19} $$

Comparing Eq. (18) with Eq. (2), Eq. (18) is a simple replacement of Eq. (2) as follows:

$$ D_i^0 \;\rightarrow\; D_i^0 + \tilde{D}_i \quad , \quad \overline{E}_i \;\rightarrow\; E_i^0 + \tilde{E}_i \quad , \quad \overline{\varepsilon}^{D} \;\rightarrow\; \varepsilon^{D} \,. \tag{20} $$

Therefore, since the following analysis is the same as that in the previous section with the replacement shown in Eq. (20), the form of obtained solutions is the same. However, it is noted that the unknown permittivity $\overline{\varepsilon}^{D}$ that appears in the coefficients L_1^{Ω} and A_1^{Ω} in Eq. (6) and the coefficients P_{11}^{Ω} and $P_{11}^{p\Omega}$ in Eq. (9) is replaced with the known permittivity ε^{D} of the matrix. From the above, referring to Eqs. (12) and (13), the macroscopic total electric field ${}^{G}\overline{\mathbf{E}}$ and the macroscopic total dielectric flux ${}^{G}\overline{\mathbf{D}}$ of the material are obtained as follows:

$$ \begin{aligned} {}^{G}\overline{\mathbf{E}} &= \frac{1}{3} f (P_{11}^{\Omega} + P_{22}^{\Omega} + P_{33}^{\Omega})({}^{G}\mathbf{E}^0 + {}^{G}\tilde{\mathbf{E}}) + (1 - f)\, {}^{G}\mathbf{E}^{m} \\ &= \left\{ \frac{1}{3} f (P_{11}^{\Omega} + P_{22}^{\Omega} + P_{33}^{\Omega}) + (1 - f) \right\} ({}^{G}\mathbf{E}^0 + {}^{G}\tilde{\mathbf{E}}) \,, \end{aligned} \tag{21} $$

$$ \begin{aligned} {}^{G}\overline{\mathbf{D}} &= \frac{1}{3} f (\varepsilon_{11}^{D\Omega} P_{11}^{\Omega} + \varepsilon_{22}^{D\Omega} P_{22}^{\Omega} + \varepsilon_{33}^{D\Omega} P_{33}^{\Omega})({}^{G}\mathbf{E}^0 + {}^{G}\tilde{\mathbf{E}}) + (1 - f)\, {}^{G}\mathbf{D}^{m} \\ &= \left\{ \frac{1}{3} f (\varepsilon_{11}^{D\Omega} P_{11}^{\Omega} + \varepsilon_{22}^{D\Omega} P_{22}^{\Omega} + \varepsilon_{33}^{D\Omega} P_{33}^{\Omega}) + (1 - f)\varepsilon^{D} \right\} ({}^{G}\mathbf{E}^0 + {}^{G}\tilde{\mathbf{E}}) \,, \end{aligned} \tag{22} $$

where ${}^{G}\mathbf{E}^{m}$ and ${}^{G}\mathbf{D}^{m}$ in the above equation are the total electric field and the total dielectric flux of the matrix. Unlike Eq. (14), these are given by the sum of the external field and the interaction field, and have the following relations:

$$ \begin{aligned} &{}^{G}E_i^{m} = {}^{G}E_i^0 + {}^{G}\tilde{E}_i \quad , \quad {}^{G}D_i^{m} = {}^{G}D_i^0 + {}^{G}\tilde{D}_i \,. \\ &{}^{G}D_i^{m} = \delta_{ij}\varepsilon^{D}\, {}^{G}E_j^{m} \quad or \quad {}^{G}\mathbf{D}^{m} = \varepsilon^{D}\, {}^{G}\mathbf{E}^{m} \,. \end{aligned} \tag{23} $$

Eq. (23) is used to derive Eqs. (21) and (22). Eliminating $({}^{G}\mathbf{E}^0 + {}^{G}\tilde{\mathbf{E}})$ in Eqs. (21) and (22) and obtaining the relation between ${}^{G}\overline{\mathbf{E}}$ and ${}^{G}\overline{\mathbf{D}}$, and equating this with Eq. (16), the effective permittivity is finally obtained as follows:

$$ \overline{\varepsilon}^{D} = \varepsilon^{D} + \frac{\dfrac{1}{3} f\, \varepsilon^{D} \left\{ \dfrac{\varepsilon_{11}^{D\Omega} - \varepsilon^{D}}{H_1^{\Omega}\varepsilon_{11}^{D\Omega} + (1 - H_1^{\Omega})\varepsilon^{D}} + \dfrac{\varepsilon_{22}^{D\Omega} - \varepsilon^{D}}{H_2^{\Omega}\varepsilon_{22}^{D\Omega} + (1 - H_2^{\Omega})\varepsilon^{D}} + \dfrac{\varepsilon_{33}^{D\Omega} - \varepsilon^{D}}{H_3^{\Omega}\varepsilon_{33}^{D\Omega} + (1 - H_3^{\Omega})\varepsilon^{D}} \right\}}{(1 - f) + \dfrac{1}{3} f\, \varepsilon^{D} \left\{ \dfrac{1}{H_1^{\Omega}\varepsilon_{11}^{D\Omega} + (1 - H_1^{\Omega})\varepsilon^{D}} + \dfrac{1}{H_2^{\Omega}\varepsilon_{22}^{D\Omega} + (1 - H_2^{\Omega})\varepsilon^{D}} + \dfrac{1}{H_3^{\Omega}\varepsilon_{33}^{D\Omega} + (1 - H_3^{\Omega})\varepsilon^{D}} \right\}} \,. \tag{24} $$

From this derivation process, in the Mori-Tanaka's theory, the effective permittivity can be obtained directly without solving the unknown interaction fields ${}^{G}\tilde{D}_i$ and ${}^{G}\tilde{E}_i$. This point differs greatly from the self-consistent method. Interaction fields ${}^{G}\tilde{D}_i$ and ${}^{G}\tilde{E}_i$ are obtained from the condition that the sum of the internal dielectric flux over the entire material is zero. ${}^{G}\overline{\mathbf{D}}$ in Eq. (22) is given by the sum of the dielectric flux acting externally ${}^{G}\mathbf{D}^0$ and the total internal dielectric flux. Therefore, the total internal dielectric flux obtained by subtracting ${}^{G}\mathbf{D}^0$ from ${}^{G}\overline{\mathbf{D}}$ must be zero. Therefore, from Eqs. (22) and (19), the interaction electric field ${}^{G}\tilde{\mathbf{E}}$ is obtained as

$$ {}^{G}\overline{\mathbf{D}} - {}^{G}\mathbf{D}^{0} = \mathbf{0} \,. $$

$$ \therefore {}^{G}\tilde{\mathbf{E}} = \frac{f\left\{1 - \frac{1}{3\varepsilon^{D}}(\varepsilon_{11}^{D\Omega} P_{11}^{\Omega} + \varepsilon_{22}^{D\Omega} P_{22}^{\Omega} + \varepsilon_{33}^{D\Omega} P_{33}^{\Omega})\right\}}{1 - f\left\{1 - \frac{1}{3\varepsilon^{D}}(\varepsilon_{11}^{D\Omega} P_{11}^{\Omega} + \varepsilon_{22}^{D\Omega} P_{22}^{\Omega} + \varepsilon_{33}^{D\Omega} P_{33}^{\Omega})\right\}} {}^{G}\mathbf{E}^{0} \,. \tag{25} $$

The interaction dielectric flux $\tilde{D}_i$ can be derived by substituting Eq. (25) into the second equation of Eq. (19).

2.3. Solutions for special cases

2.3.1. A case where the physical property of the filler is isotropic and its shape is spheroidal

In this section, by using the solutions obtained in Sections 2.1 and 2.2, we show the solution for the special case where the physical property of the filler is isotropic and its shape is spheroidal. In this case, since $\varepsilon_{11}^{D\Omega} = \varepsilon_{22}^{D\Omega} = \varepsilon_{33}^{D\Omega} = \varepsilon^{D\Omega}$ and $H_1^{\Omega} = H_2^{\Omega} = (1 - H_3^{\Omega})/2$ (see Appendix A) hold, substituting these into solutions of the self-consistent method and the Mori-Tanaka's theory, Eqs. (17) and (24), respectively, we have

self-consistent method:

$$ \overline{\varepsilon}^{D} = \varepsilon^{D} + f\,\overline{\varepsilon}^{D}(\varepsilon^{D\Omega} - \varepsilon^{D})\left\{ \frac{2}{(\varepsilon^{D\Omega} + 2\overline{\varepsilon}^{D}) + \frac{1}{2}(1 - 3H_3^{\Omega})(\varepsilon^{D\Omega} - \overline{\varepsilon}^{D})} + \frac{1}{(\varepsilon^{D\Omega} + 2\overline{\varepsilon}^{D}) - (1 - 3H_3^{\Omega})(\varepsilon^{D\Omega} - \overline{\varepsilon}^{D})} \right\} , \tag{26a} $$

Mori-Tanaka's theory:

$$ \overline{\varepsilon}^{D} = \varepsilon^{D} + \frac{3f\varepsilon^{D}(\varepsilon^{D\Omega} - \varepsilon^{D})}{\frac{(1-f)\left\{(\varepsilon^{D\Omega} + 2\varepsilon^{D}) + \frac{1}{2}(\varepsilon^{D\Omega} - \varepsilon^{D})(1 - 3H_3^{\Omega})\right\}\left\{(\varepsilon^{D\Omega} + 2\varepsilon^{D}) - (\varepsilon^{D\Omega} - \varepsilon^{D})(1 - 3H_3^{\Omega})\right\}}{(\varepsilon^{D\Omega} + 2\varepsilon^{D}) - \frac{1}{2}(\varepsilon^{D\Omega} - \varepsilon^{D})(1 - 3H_3^{\Omega})} + 3f\varepsilon^{D}} \,. \tag{26b} $$

The same solution expressed in a slightly different form from Eq. (26b) was derived by Hatta et al. [10]. Furthermore, when the shape of the filler is spherical, $H_3^{\Omega} = 1/3$ holds (see Appendix A), so substituting this into Eq. (26) eliminates the term $1 - 3H_3^{\Omega}$, and we find immediately to be as follows:

$$ \text{self-consistent method:} \quad \overline{\varepsilon}^{D} = \varepsilon^{D} + \frac{3f\overline{\varepsilon}^{D}(\varepsilon^{D\Omega} - \varepsilon^{D})}{3\overline{\varepsilon}^{D} + (\varepsilon^{D\Omega} - \overline{\varepsilon}^{D})} \,, \tag{27a} $$

$$ \text{Mori-Tanaka's theory:} \quad \overline{\varepsilon}^{D} = \varepsilon^{D} + \frac{3f\varepsilon^{D}(\varepsilon^{D\Omega} - \varepsilon^{D})}{3\varepsilon^{D} + (1 - f)(\varepsilon^{D\Omega} - \varepsilon^{D})} \,. \tag{27b} $$

The solution of Eq. (27a) is in agreement with that derived by Kanaun et al. [13].

2.3.2. A case where the filler is a void

In this section, we consider the case where all fillers are voids and the inside is filled with air. The permittivity of air is almost equal to that of vacuum ε^{0}. Therefore, the effective permittivity can be obtained by substituting $\varepsilon^{D\Omega} = \varepsilon^{0}$ in Eq. (27).

The solutions of effective permittivity given by Eqs. (17), (24), (26), and (27) can be applied to problems of thermal conduction, electrical conduction, and magnetism. Therefore, it is possible to obtain solutions of effective thermal conductivity, electrical conductivity, and magnetic permeability from that of effective permittivity. For example, the solution of effective thermal conductivity can be obtained by simply replacing the symbol ε^{D} with the symbol k for thermal conductivity in these equations. Using this analogy, we consider the effective thermal conductivity, magnetic permeability, and electrical conductivity when the filler is void and filled with air. A foam metal is one such material. In this material, the thermal conductivity of the metal matrix is more than 10^4 times that of air, the magnetic permeability of the matrix is more than 10^5 times that of air, and the electrical conductivity is on the order of even greater. For the thermal conductivity of such foam metal, $k^{\Omega} = 0$ holds approximately. Thus, when the thermal conductivity inside the voids is sufficiently small compared to that of the matrix and can be regarded as zero, the effective thermal conductivity $\overline{k}$ can be expressed approximately as follows:

$$ \text{self-consistent method:} \quad \overline{k} = k - \frac{1}{3}fk\left(\frac{1}{1 - H_1^{\Omega}} + \frac{1}{1 - H_2^{\Omega}} + \frac{1}{1 - H_3^{\Omega}}\right) , \tag{28a} $$

$$ \text{Mori-Tanaka's theory:} \quad \overline{k} = k - \frac{\frac{1}{3}fk\left(\frac{1}{1 - H_1^{\Omega}} + \frac{1}{1 - H_2^{\Omega}} + \frac{1}{1 - H_3^{\Omega}}\right)}{(1 - f) + \frac{1}{3}f\left(\frac{1}{1 - H_1^{\Omega}} + \frac{1}{1 - H_2^{\Omega}} + \frac{1}{1 - H_3^{\Omega}}\right)} \,, \tag{28b} $$

where k is the thermal conductivity of the matrix. It is interesting that the solution of self-consistent method Eq. (28a), like that of Mori-Tanaka's theory Eq. (28b), reduces to be an explicit expression. This approximate solution can also be applied to electrical conductivity and magnetic permeability for the reason mentioned above.

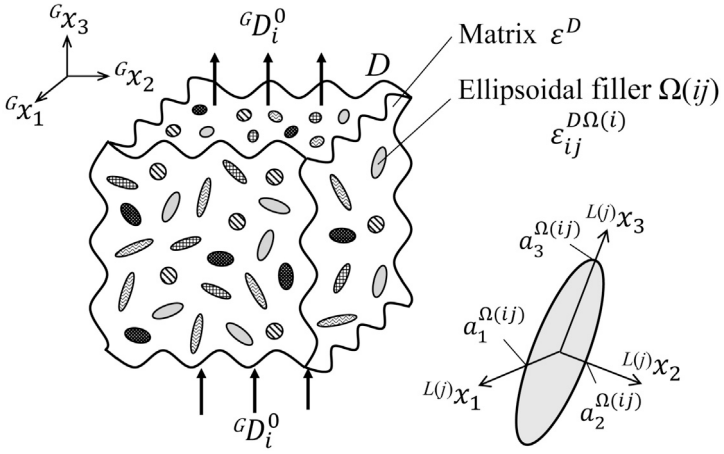

Fig. 5. Composite material containing many ellipsoidal fillers with different physical properties and shapes oriented randomly. If there is no matrix, it becomes a polycrystalline material.

3. Analysis for composite materials (or polycrystalline materials) containing many kinds of fillers (or crystal grains) oriented randomly

3.1. Analytical model

Fig. 5 shows a composite material in which many kinds of ellipsoidal fillers (or crystal grains) with different physical properties and shapes are oriented randomly. The fillers are classified by (i) in terms of their physical properties and shapes. To express this classification, (i) is added to the right shoulder of the dielectric constant $\varepsilon_{ij}^{D\Omega(i)}$ as shown in Fig. 5. Assume that there are n types of such fillers. Although not shown in Fig. 5, the eigen electric field is similarly classified by (i) and expressed as $E_i^{p\Omega(i)}$. It is assumed that the fillers are classified by (j) in terms of their orientations and there are m types. Since all fillers are oriented randomly, there are m types of orientations for all (i)th fillers. The filler region with physical property and shape (i) and orientation (j) is represented by $\Omega(ij)$, and the volume fraction of $\Omega(ij)$ is $f_{(ij)}$. As in the previous chapter, if the total volume fraction of all fillers is f, then $f = \sum_{i=1}^{n} \sum_{j=1}^{m} f_{(ij)}$. In addition, the model in Fig. 5 becomes to be a polycrystalline material when the matrix does not exist.

3.2. Analysis of effective permittivity by the self-consistent method

As shown in Chap.2, the region around a filler $\Omega(ij)$ is smeared out with a material of unknown effective permittivity $\bar{\varepsilon}^D$. The equivalent equation is solved in the local coordinate system ${}^{L(j)}x_i$ taken along the direction of the principal semi-axis of $\Omega(ij)$, then the total electric field and the total dielectric flux of $\Omega(ij)$ can be derived as follows by referring to Eqs. (7b) and (8b).

$$ {}^{L(j)}\mathbf{E}^{total} = \mathbf{P}^{\Omega(i)}\ {}^{L(j)}\overline{\mathbf{E}} - \mathbf{P}^{p\Omega(i)}\,\mathbf{E}^{p\Omega(i)}\,, \tag{29b} $$

$$ {}^{L(j)}\mathbf{D}^{total} = \boldsymbol{\varepsilon}^{D\Omega(i)}\left({}^{L(j)}\mathbf{E}^{total} - \mathbf{E}^{p\Omega(i)}\right) = \boldsymbol{\varepsilon}^{D\Omega(i)}\left\{\mathbf{P}^{\Omega(i)}\ {}^{L(j)}\overline{\mathbf{E}} - (\mathbf{P}^{p\Omega(i)} - \mathbf{I})\mathbf{E}^{p\Omega(i)}\right\}, \tag{30b} $$

where $\mathbf{P}^{\Omega(i)}$ and $\mathbf{P}^{p\Omega(i)}$ are coefficients obtained by adding (i) to their right shoulders of the coefficients in Eq. (9).

Eqs. (29b) and (30b) are transformed into the global coordinate system from Eqs. (7c) and (8c) as follows:

$$ {}^{G}\mathbf{E}^{total} = \{\boldsymbol{l}^{(j)}\}^{-1}\ \mathbf{P}^{\Omega(i)}\ \boldsymbol{l}^{(j)}\ {}^{G}\overline{\mathbf{E}} - \{\boldsymbol{l}^{(j)}\}^{-1}\ \mathbf{P}^{p\Omega(i)}\mathbf{E}^{p\Omega(i)}\,, \tag{29c} $$

$$ {}^{G}\mathbf{D}^{total} = \{\boldsymbol{l}^{(j)}\}^{-1}\ \boldsymbol{\varepsilon}^{D\Omega}\ \mathbf{P}^{\Omega(i)}\ \boldsymbol{l}^{(j)}\ {}^{G}\overline{\mathbf{E}} - \{\boldsymbol{l}^{(j)}\}^{-1}\ \boldsymbol{\varepsilon}^{D\Omega}\ (\mathbf{P}^{p\Omega(i)} - \mathbf{I})\mathbf{E}^{p\Omega(i)}\,. \tag{30c} $$

Using Eqs. (29c) and (30c), take the summation of total electric fields and total dielectric fluxes of all fillers and matrix. Referring to Eqs. (12) and (13), the macroscopic total electric field ${}^{G}\overline{\mathbf{E}}$ and the macroscopic total dielectric flux ${}^{G}\overline{\mathbf{D}}$ of the material are given by

$$ \begin{aligned} {}^{G}\overline{\mathbf{E}} &= \sum_{i=1}^{n}\sum_{j=1}^{m} f_{(ij)}\ {}^{G}\mathbf{E}^{total} + \left(1 - \sum_{i=1}^{n}\sum_{j=1}^{m} f_{(ij)}\right){}^{G}\mathbf{E}^{m} \\ &= \sum_{i=1}^{n} \frac{f_{(i)}}{8\pi^2} \int_0^{\pi}\int_0^{2\pi}\int_0^{2\pi} sin\theta \left(\boldsymbol{l}^{-1}\ \mathbf{P}^{\Omega(i)}\ \boldsymbol{l}\ {}^{G}\overline{\mathbf{E}} - \boldsymbol{l}^{-1}\ \mathbf{P}^{p\Omega(i)}\mathbf{E}^{p\Omega(i)}\right) d\theta\, d\phi\, d\psi + (1-f)\,{}^{G}\mathbf{E}^{m} \\ &= \frac{1}{3}\sum_{i=1}^{n} f_{(i)}(P_{11}^{\Omega(i)} + P_{22}^{\Omega(i)} + P_{33}^{\Omega(i)})\,{}^{G}\overline{\mathbf{E}} + (1-f)\,{}^{G}\mathbf{E}^{m}\,, \end{aligned} \tag{31} $$

$$
\begin{aligned}
{}^{G}\overline{\mathbf{D}} &= \sum_{i=1}^{n}\sum_{j=1}^{m} f_{(ij)}\,{}^{G}\mathbf{D}^{total} + \Big(1-\sum_{i=1}^{n}\sum_{j=1}^{m} f_{(ij)}\Big){}^{G}\mathbf{D}^{m} \\
&= \sum_{i=1}^{n}\frac{f_{(i)}}{8\pi^2}\int_0^{\pi}\int_0^{2\pi}\int_0^{2\pi} sin\theta\Big\{ I^{-1}\boldsymbol{\varepsilon}^{D\Omega(i)}\,\mathbf{P}^{\Omega(i)}\,I\,{}^{G}\overline{\mathbf{E}} - I^{-1}\boldsymbol{\varepsilon}^{D\Omega(i)}\,(\mathbf{P}^{p\Omega(i)}-\mathbf{I})\mathbf{E}^{p\Omega(i)}\Big\}d\theta\,d\phi\,d\psi + (1-f)\,{}^{G}\mathbf{D}^{m} \\
&= \frac{1}{3}\sum_{i=1}^{n} f_{(i)}(\varepsilon_{11}^{D\Omega(i)}P_{11}^{\Omega(i)} + \varepsilon_{22}^{D\Omega(i)}P_{22}^{\Omega(i)} + \varepsilon_{33}^{D\Omega(i)}P_{33}^{\Omega(i)})\,{}^{G}\overline{\mathbf{E}} + (1-f)\,{}^{G}\mathbf{D}^{m}\,,
\end{aligned}
\tag{32}
$$

where $f_{(i)} = \sum_{j=1}^{m} f_{(ij)}$ holds for the volume fraction. From Eqs. (31), (32), and (14), the relation between ${}^{G}\overline{\mathbf{E}}$ and ${}^{G}\overline{\mathbf{D}}$ can be obtained. Equating this relation with Eq. (16), the effective permittivity $\overline{\varepsilon}^{D}$ is finally obtained as

$$
\overline{\varepsilon}^{D} = \varepsilon^{D} + \frac{\overline{\varepsilon}^{D}}{3}\sum_{i=1}^{n} f_{(i)}\left\{ \frac{\varepsilon_{11}^{D\Omega(i)}-\varepsilon^{D}}{H_1^{\Omega(i)}\varepsilon_{11}^{D\Omega(i)}+(1-H_1^{\Omega(i)})\overline{\varepsilon}^{D}} + \frac{\varepsilon_{22}^{D\Omega(i)}-\varepsilon^{D}}{H_2^{\Omega(i)}\varepsilon_{22}^{D\Omega(i)}+(1-H_2^{\Omega(i)})\overline{\varepsilon}^{D}} + \frac{\varepsilon_{33}^{D\Omega(i)}-\varepsilon^{D}}{H_3^{\Omega(i)}\varepsilon_{33}^{D\Omega(i)}+(1-H_3^{\Omega(i)})\overline{\varepsilon}^{D}} \right\}. \tag{33}
$$

Eq. (33) is the solution for multiphase composites. In the case of polycrystalline materials, since ${}^{G}\mathbf{D}^{m}$ and ${}^{G}\mathbf{E}^{m}$ are zero or $f = 1$ in Eqs. (31) and (32), we have

$$
\overline{\varepsilon}^{D} = \frac{\overline{\varepsilon}^{D}}{3}\sum_{i=1}^{n} f_{(i)}\left\{ \frac{\varepsilon_{11}^{D\Omega(i)}}{H_1^{\Omega(i)}\varepsilon_{11}^{D\Omega(i)}+(1-H_1^{\Omega(i)})\overline{\varepsilon}^{D}} + \frac{\varepsilon_{22}^{D\Omega(i)}}{H_2^{\Omega(i)}\varepsilon_{22}^{D\Omega(i)}+(1-H_2^{\Omega(i)})\overline{\varepsilon}^{D}} + \frac{\varepsilon_{33}^{D\Omega(i)}}{H_3^{\Omega(i)}\varepsilon_{33}^{D\Omega(i)}+(1-H_3^{\Omega(i)})\overline{\varepsilon}^{D}} \right\}. \tag{34}
$$

In Eq. (34), if there is only one kind of filler and it is isotropic, that is, in the case of $n = 1$ and $\varepsilon_{11}^{D\Omega} = \varepsilon_{22}^{D} = \varepsilon_{33}^{D\Omega} = \varepsilon^{D\Omega}$, then $\overline{\varepsilon}^{D}$ that satisfies Eq. (34) is the only $\varepsilon^{D\Omega}$. Therefore, it can be seen that Eq. (34) is a physically consistent solution.

3.3. Analysis of effective permittivity by the Mori-Tanaka's theory

Similar to Section 3.2, we can perform the replacement shown in Eqs. (20) and (23). Therefore, from Eqs. (31) and (32), the macroscopic total electric field ${}^{G}\overline{\mathbf{E}}$ and the macroscopic total dielectric flux ${}^{G}\overline{\mathbf{D}}$ of the material are given by

$$
{}^{G}\overline{\mathbf{E}} = \Big\{ \frac{1}{3}\sum_{i=1}^{n} f_{(i)}(P_{11}^{\Omega(i)} + P_{22}^{\Omega(i)} + P_{33}^{\Omega(i)}) + (1-f) \Big\}({}^{G}\mathbf{E}^{0} + {}^{G}\tilde{\mathbf{E}})\,, \tag{35}
$$

$$
{}^{G}\overline{\mathbf{D}} = \Big\{ \frac{1}{3}\sum_{i=1}^{n} f_{(i)}(\varepsilon_{11}^{D\Omega(i)}P_{11}^{\Omega(i)} + \varepsilon_{22}^{D\Omega(i)}P_{22}^{\Omega(i)} + \varepsilon_{33}^{D\Omega(i)}P_{33}^{\Omega(i)}) + (1-f)\varepsilon^{D} \Big\}({}^{G}\mathbf{E}^{0} + {}^{G}\tilde{\mathbf{E}})\,. \tag{36}
$$

Eliminating $({}^{G}\mathbf{E}^{0} + {}^{G}\tilde{\mathbf{E}})$ in Eqs. (35) and (36) and deriving the relation between ${}^{G}\overline{\mathbf{E}}$ and ${}^{G}\overline{\mathbf{D}}$, and equating this with Eq. (16), the effective permittivity is finally obtained as

$$
\overline{\varepsilon}^{D} = \varepsilon^{D} + \frac{\dfrac{\varepsilon^{D}}{3}\displaystyle\sum_{i=1}^{n} f_{(i)}\left\{ \frac{\varepsilon_{11}^{D\Omega(i)}-\varepsilon^{D}}{H_1^{\Omega(i)}\varepsilon_{11}^{D\Omega(i)}+(1-H_1^{\Omega(i)})\varepsilon^{D}} + \frac{\varepsilon_{22}^{D\Omega(i)}-\varepsilon^{D}}{H_2^{\Omega(i)}\varepsilon_{22}^{D\Omega(i)}+(1-H_2^{\Omega(i)})\varepsilon^{D}} + \frac{\varepsilon_{33}^{D\Omega(i)}-\varepsilon^{D}}{H_3^{\Omega(i)}\varepsilon_{33}^{D\Omega(i)}+(1-H_3^{\Omega(i)})\varepsilon^{D}} \right\}}{(1-f) + \dfrac{\varepsilon^{D}}{3}\displaystyle\sum_{i=1}^{n} f_{(i)}\left\{ \frac{1}{H_1^{\Omega(i)}\varepsilon_{11}^{D\Omega(i)}+(1-H_1^{\Omega(i)})\varepsilon^{D}} + \frac{1}{H_2^{\Omega(i)}\varepsilon_{22}^{D\Omega(i)}+(1-H_2^{\Omega(i)})\varepsilon^{D}} + \frac{1}{H_3^{\Omega(i)}\varepsilon_{33}^{D\Omega(i)}+(1-H_3^{\Omega(i)})\varepsilon^{D}} \right\}}. \tag{37}
$$

In the case of polycrystalline materials, since there is no matrix, substituting $f = 1$ and taking the limit $\varepsilon^{D} \to 0$ for Eq. (37), we have

$$
\overline{\varepsilon}^{D} = \frac{\displaystyle\sum_{i=1}^{n} f_{(i)}\left(\frac{1}{H_1^{\Omega(i)}} + \frac{1}{H_2^{\Omega(i)}} + \frac{1}{H_3^{\Omega(i)}} \right)}{\displaystyle\sum_{i=1}^{n} f_{(i)}\left(\frac{1}{H_1^{\Omega(i)}\varepsilon_{11}^{D\Omega(i)}} + \frac{1}{H_2^{\Omega(i)}\varepsilon_{22}^{D\Omega(i)}} + \frac{1}{H_3^{\Omega(i)}\varepsilon_{33}^{D\Omega(i)}} \right)}. \tag{38}
$$

In Eq. (38), if there is only one kind of filler and it is isotropic ($\varepsilon_{11}^{D\Omega} = \varepsilon_{22}^{D\Omega} = \varepsilon_{33}^{D\Omega} = \varepsilon^{D\Omega}$), then $\overline{\varepsilon}^{D} = \varepsilon^{D\Omega}$. Therefore, it can be seen that Eq. (38) is a physically consistent solution like Eq. (34).

4. Numerical calculations and discussions

4.1. Material properties of constituents used in calculations

In this section, using the solutions obtained in Sections 2 and 3, the effective thermal conductivity of composites containing randomly oriented ellipsoidal fillers is calculated. In this calculation, we assume the same constituents used in the experiments by Agari et al. [22] [23]. In their experiments, polyethylene is used as a matrix, and short carbon fibers or quartz particles are used as

Table 1
Thermal conductivity of constituents.

	Material	Thermal conductivity (W/(m · K))	
Filler	Carbon (PAN-based)*1	4.00	
	Carbon (PAN-based)*3	axial	1.60
		radial	0.17
	Quartz (16 μm)*2	9.64	
	Quartz (156 μm)*2	5.87	
Matrix	Polyethylene*1,*2	0.28	

*1 [23], *2 [22], *3 [17].

Table 2
Combination of constituents of composite materials.

	Filler (& Void)	Matrix
Isotropic filler	Carbon (PAN-based)*1	Polyethylene
	Quartz (156 μm)*2	
	Quartz (156 μm)*2 & Void	
	Quartz (156 μm)*2 & Quartz (16 μm)	
	Quartz (156 μm)*2 & Quartz (16 μm) & Void	
Anisotropic filler	Carbon (PAN-based)*3	

fillers. The thermal conductivities of these materials are shown in Table 1. Agari et al. assume that all of the constituents are isotropic materials. As shown in Table 1, the thermal conductivity of quartz particles differs depending on their particle size. Table 2 shows the combinations of constituents of composite materials used in the calculations. For quartz particles, we deal with two types of composite materials. One is a material containing particles with a diameter of 156 μm, and the other is a hybrid material containing two types of particles with diameters of 156 μm and 16 μm. These composite materials are made by impregnating the gaps among particles with resin. If the resin impregnation is not successful, gaps will remain as voids. So calculations are also performed for the case including voids.

Table 1 lists two types of PAN-based carbon fibers with different thermal conductivity. It is a well-known fact that carbon fibers are generally anisotropic materials with different physical properties in the longitudinal (axial) direction of fiber and the radial direction perpendicular to the fiber axis [17] [18]. However, there are few studies that clarify the anisotropic properties of fillers and investigate the effects of these anisotropic properties on the effective physical properties of composite materials. That is, most studies assume that the properties of fillers are isotropic. Therefore, in this study, as shown in Table 2, we also assume a composite material containing anisotropic PAN-based carbon fillers in the polyethylene resin matrix and investigate the coupling effect of the shape and the anisotropy of the fillers on the effective thermal conductivity of composites.

For composite materials shown in Table 2, the analytical results of effective thermal conductivity are compared with the experimental ones. Hashin and Shtrikman obtained the upper and lower bounds of the effective permeability by using the variational method [8]. In their analysis, the shape of each phase is arbitrary and the effective physical properties of the entire material are assumed to be isotropic. We also compare the present results with the upper and lower bound of Hashin et al.

4.2. Analytical results of effective thermal conductivity

4.2.1. The case of isotropic filler

Fig. 6 shows analytical results of the effective thermal conductivity $\overline{k}$ for the isotropic carbon filler / polyethylene material. This calculation is performed under the condition that the aspect ratio is continuously changed for each shape of the filler shown in Fig. A (see Appendix A) while keeping the volume fraction of fillers f constant at 0.15. Fig. 6(a), (b), and (c)~(e) correspond to a longitudinal elliptic flake, a longitudinal elliptic cylinder, and a spheroid, respectively. The vertical axis of the figure is $\overline{k}/k$, which is dimensionless with the thermal conductivity of matrix k, and the horizontal axis is the aspect ratio of the filler ω_3. The red line and the blue line show the result of the self-consistent method (denoted by SC) and the Mori-Tanaka's theory (denoted by MT). Open circles, open rectangles, solid circles, and open triangles in Fig. 6(c) and (d) are the experimental results obtained by Agari et al.

The solution of the lower and upper bounds of the effective permeability of multiphase composites obtained by Hashin and Shtrikman [8] can be expressed as the solution of thermal conductivity $\overline{k}^{(-)}$ and $\overline{k}^{(+)}$ by the analogy between magnetism and heat conduction, as follows:

$$\overline{k}^{(-)} = k_1 + \frac{A_1}{1 - \dfrac{A_1}{3k_1}} \quad , \quad \overline{k}^{(+)} = k_m + \frac{A_m}{1 - \dfrac{A_m}{3k_m}} \, , \tag{39a}$$

$$A_1 = \sum_{i=2}^{m} \frac{f_i}{\dfrac{1}{k_i - k_1} + \dfrac{1}{3k_1}} \quad , \quad A_m = \sum_{i=1}^{m-1} \frac{f_i}{\dfrac{1}{k_i - k_m} + \dfrac{1}{3k_m}} \, , \tag{39b}$$

where k_i is the thermal conductivity of the ith phase assumed to be an isotropic material, and k_1 and k_m represent the minimum and maximum thermal conductivities, respectively. In the special case of a two-phase material, Eq. (39) reduces to

$$\overline{k}^{(-)} = k_1 + \frac{f_2}{\dfrac{1}{k_2 - k_1} + \dfrac{f_1}{3k_1}} \quad , \quad \overline{k}^{(+)} = k_2 + \frac{f_1}{\dfrac{1}{k_1 - k_2} + \dfrac{f_2}{3k_2}} \quad , \quad (k_1 < k_2) \, . \tag{40}$$

The results of upper and lower bounds expressed by Eq. (40) are indicated by dashed lines (HS(+), HS(−)) in Fig. 6. From the figure, it can be seen that the results of SC and MT always exist between the upper and lower bounds regardless of the aspect ratio of the filler ω_3. The result of SC is higher than that of MT for any aspect ratio. Fig. 6(c)~(e) shows that the results of SC and MT asymptotically approach the upper bound, as ω_3 decreases and the shape of the filler becomes flatter. When the shape of the

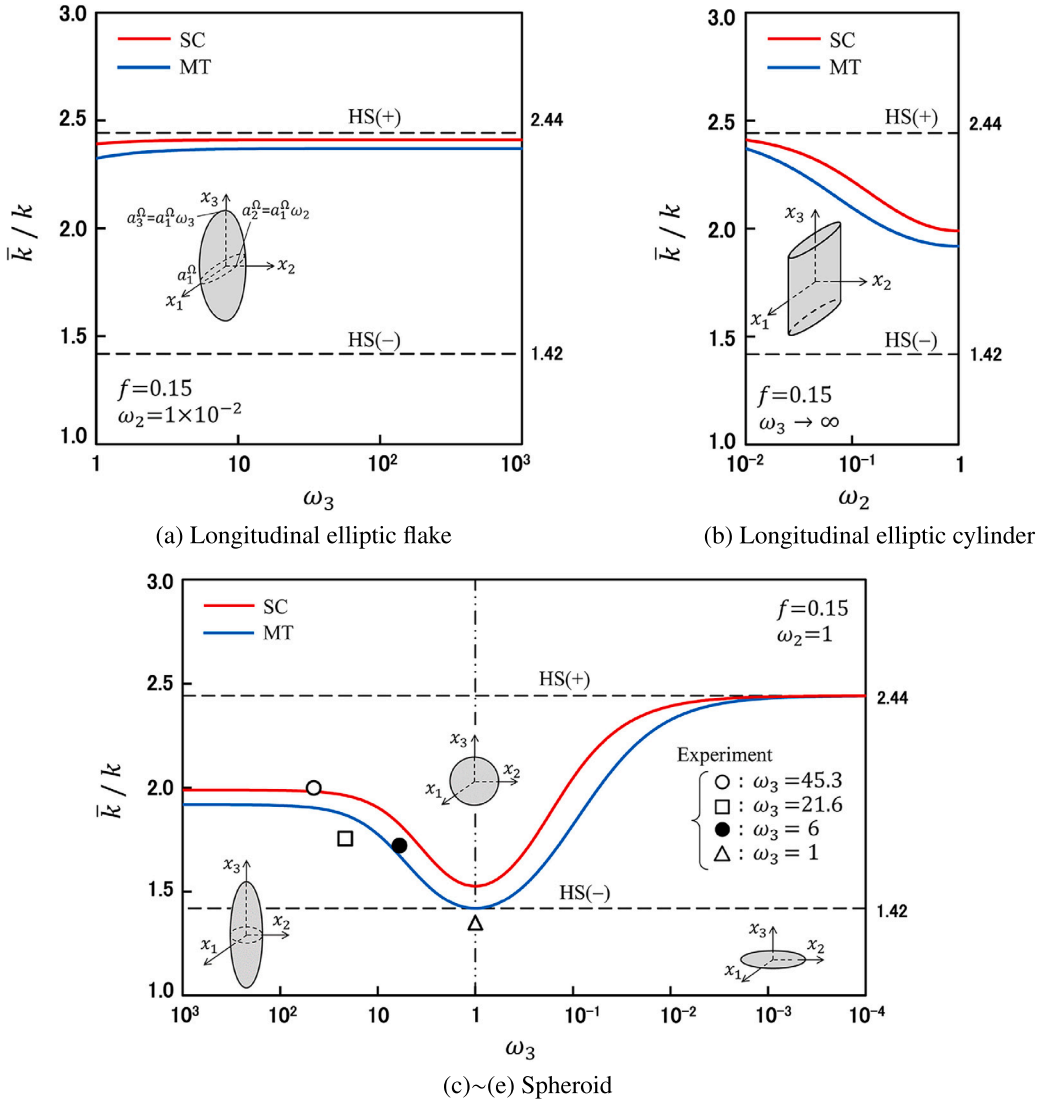

Fig. 6. Change in effective thermal conductivity $\bar{k}$ of isotropic carbon (PAN-based)*[1] / Polyethylene with the aspect ratio of filler. (a), (b), and (c)-(e) show the results when the shape of the filler is a longitudinal elliptic flake, longitudinal elliptic cylinder, and spheroid, respectively. The red line and the blue one are the results of the self-consistent method and the Mori-Tanaka's theory for the three-dimensional random orientation of fillers, respectively. The dashed lines are the Hashin-Shtrikman's bounds. In Figures (c) and (d), the experimental results obtained by Agari et al. are also shown by open circles, open rectangles, solid circles, and open triangles.

filler is spherical, the result of MT becomes the same as that of the lower bound, since Eq. (27b) agrees with the lower bound of Eq. (40) replacing Eq. (27b) with the solution of the effective thermal conductivity and applying $k^{\Omega} \to k_2$ and $k \to k_1$. In addition, it is interesting that the value of $\bar{k}$ when the shape of filler is an oblate spheroid (Fig. 6(e)) or longitudinal elliptic flake (Fig. 6(a)) is about 20% higher than that of long fiber (Fig. 6(c)). In other words, if you want to increase the thermal conductivity of composite material, flat-shaped fillers are more advantageous than simple circular cross-sectioned fibers that are widely available in the market. This fact also suggests that it is possible to significantly reduce the volume fraction of fillers by devising the shape of the filler to obtain the desired value of thermal conductivity.

Next, we consider the reason why the thermal conductivity is higher when flat-shaped fillers are used rather than fibrous-shaped ones. In the case of fibrous-shaped filler, heat conduction is high only in the longitudinal direction of the fiber. On the other hand, when the shape of the filler is flat, the heat conduction in two directions in its flat plane is improved at the same time. When the flat-shaped fillers are oriented randomly, this characteristic appears in any direction. Therefore, it is considered that the thermal conductivity is higher when the shape of the filler is oblate spheroid or elliptical flake than fibrous shape.

Comparing the analytical results with the experimental ones in Fig. 6(c) and (d), it can be seen that the experimental results are almost close to the results of SC and MT. Fig. 7 shows the change in effective thermal conductivity $\bar{k}$ with the volume fraction of the filler f. Fig. 7(I) shows the result of the self-consistent method, and Fig. 7(II) that of the Mori-Tanaka's theory. The shape of the filler is spheroid, and the results of SC and MT are compared with the experimental results [23] for each aspect ratio of $\omega_3 = 45.3$,

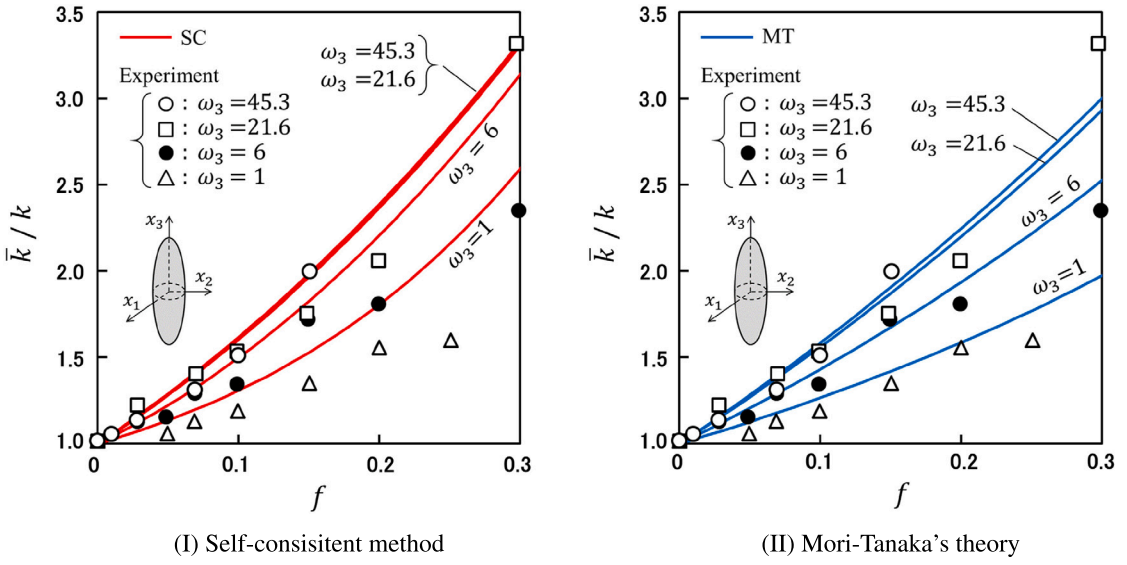

Fig. 7. Change in effective thermal conductivity $\bar{k}$ of isotropic carbon (PAN-based)*1 / Polyethylene with the volume fraction of carbon fillers f. The shape of the filler is spheroid. The results of the self-consistent method (red lines in (I)) and the Mori-Tanaka's theory (blue lines in (II)) are compared with the experimental results obtained by Agari et al. for each value of aspect ratio ω_3 = 45.3, 21.6, 6, and 1 (denoted by open circles, open rectangles, solid circles, and open triangles respectively).

21.6, 6 and 1. The line types and symbols in these figures are the same as in Fig. 6. From the figures, regardless of the aspect ratio ω_3, the effective thermal conductivity of SC is higher than that of MT even if the volume fraction of the filler is changed. This difference between SC and MT is clearly due to the difference in the evaluation of interaction among fillers. When the aspect ratio of the filler is $\omega_3 = 45.3$, the experimental results are closer to the results of SC, and MT is underestimated. However, when the aspect ratio decreases and the shape of the filler becomes a sphere of $\omega_3 = 1$, the experimental results are closer to the result of MT than that of SC, regardless of the volume fraction of the filler. From the above results, although there is some variation in the experimental data for aspect ratios from $\omega_3 = 1$ to $\omega_3 = 45.3$, the experimental results tend to be closer to the result of MT than that of SC as the aspect ratio decreases. To investigate this point further, the analysis for the quartz particles / polyethylene material (shown in Table 2) is performed. Fig. 8 shows the change in effective thermal conductivity $\bar{k}$ with the volume fraction of the filler f, for the case that quartz particles with a size of 156 μm are included in the material. Open triangles in the figure are the experimental results obtained by Agari et al. As shown in Table 2, the effective thermal conductivity is calculated for both materials with and without voids. Fig. 8(I) is the result when there are no voids in the material, and Fig. 8(II) is the result when the existence of voids is considered. In Fig. 8(I), as mentioned in Fig. 6, the result of MT completely agrees with that of the lower bound HS(−) regardless of the value of f. As the value of f increases, there is no significant difference between the results of SC and MT up to around $f = 0.2$. As the value of f increases from this point, this difference increases. However, as the value of f approaches 1, this difference decreases, and at $f = 1$, the result of SC agrees with that of MT. For the effective elastic modulus, a similar result is obtained that the difference between the results of SC and MT is small when the volume fraction of the filler is relatively small [24]. Although the types of effective physical properties are different, the fact that the tendency is the same for the volume fraction of the filler supports the fact that the results of this analysis are physically valid.

Fig. 8(II) shows the change in the effective thermal conductivity when the volume fraction of voids f_{void} is changed as a parameter. From this figure, regardless of the value of f_{void}, the value of SC is larger than that of MT, and this tendency is the same as in Fig. 7. As f_{void} increases, the values of SC and MT naturally decrease. From Figs. 8(I) and (II), comparing these analytical results with the experimental ones, the experimental results are close to the result of MT when $f_{void} = 0$.

Similar to Fig. 8, Fig. 9 shows the result of the effective thermal conductivity for a polyethylene matrix containing quartz particles with sizes 156 μm and 16 μm. Two types of quartz particles, 156 μm and 16 μm, have a volume fraction ratio of 4 : 1. Note that this calculation cannot take into account the difference between the two particle sizes. Comparing Fig. 9 with Fig. 8, the tendency of SC and MT for f and f_{void} are the same in both figures. It can be seen that the experimental results are close to the MT results for $f_{void} = 0$ even at a high volume fraction exceeding $f = 0.5$.

From the above analytical results, it is proved that the composite material prepared by Agari et al. has almost no voids and is impregnated with resin throughout the material. Furthermore, from the results in Figs. 6 to 8, it is found that the experimental results are closer to the results of MT than that of SC when the shape of the filler is spherical.

4.2.2. The case of anisotropic filler

Fig. 10 shows the change in the effective thermal conductivity $\bar{k}$ of the anisotropic carbon (PAN-based) filler / polyethylene material with the aspect ratio of the filler. In this calculation, the shape of the carbon filler is spheroidal, and the thermal conductivity of the filler in the axial direction (x_3 axis of the filler) is different from that in the radial one (x_1 or x_2 axis of the filler) as shown

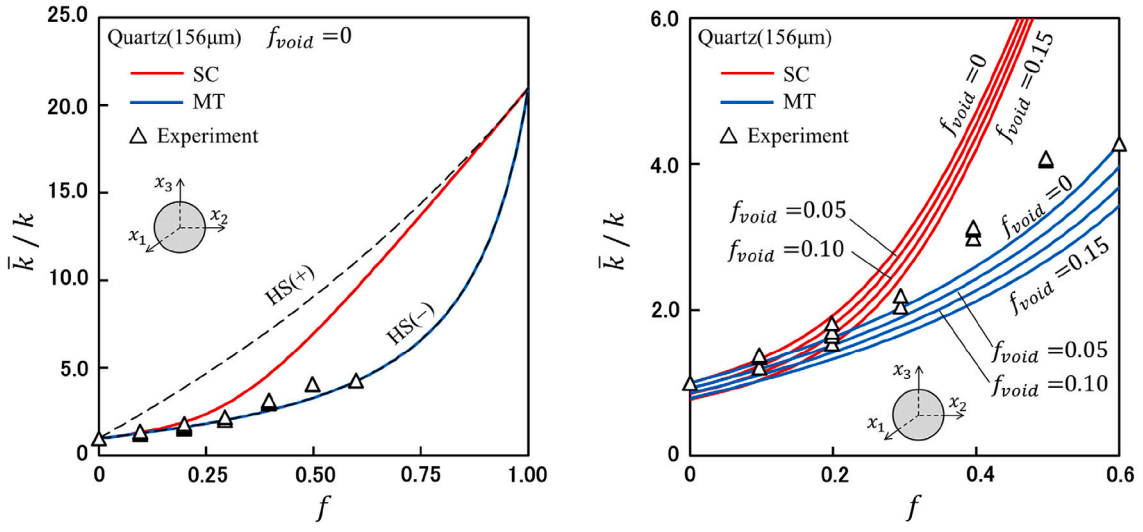

Fig. 8. Change in effective thermal conductivity $\bar{k}$ of isotropic quartz particle (156 μm)*2 / Polyethylene with the volume fraction of quartz particles f. Fig. 8(I) is the result when there are no voids in the material. Fig. 8(II) is the result when the existence of voids is considered and the volume fraction of voids f_{void} is a parameter. The shape of particles and voids is spherical ($\omega_3 = 1$). The results of the self-consistent method (red lines) and the Mori-Tanaka's theory (blue lines) are compared with the experimental results obtained by Agari et al. (open triangles).

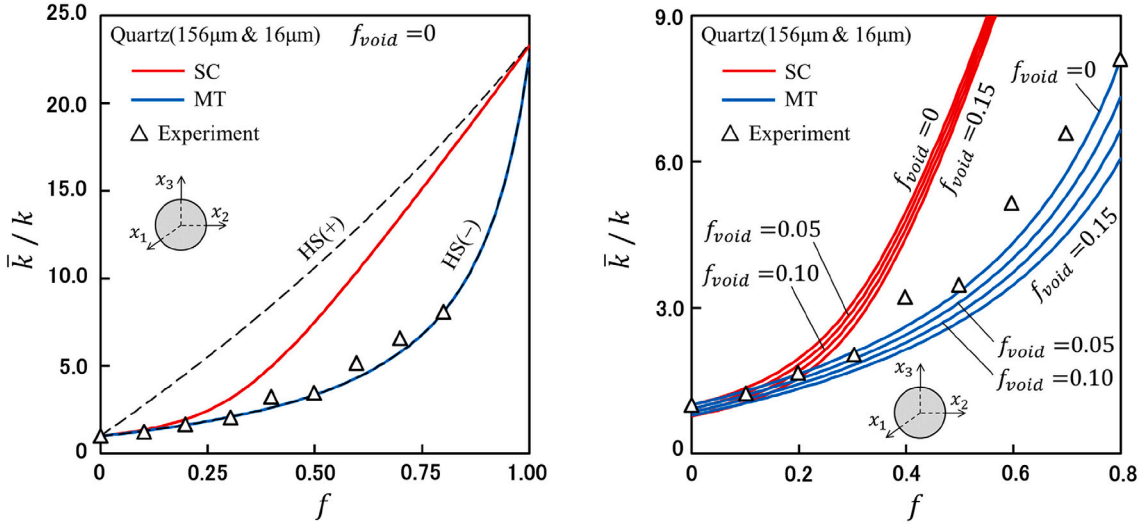

Fig. 9. Change in effective thermal conductivity $\bar{k}$ of isotropic quartz particles (156 μm and 16 μm)*2 / Polyethylene with the volume fraction of quartz particles f. The ratio of volume fraction is 156 μm : 16 μm = 4 : 1. Fig. 9(I) is the result when there are no voids in the material. Fig. 9(II) is the result when the existence of voids is considered and the volume fraction of voids f_{void} is a parameter. The shape of particles and voids is spherical ($\omega_3 = 1$). The results of the self-consistent method (red lines) and the Mori-Tanaka's theory (blue lines) are compared with the experimental results obtained by Agari et al. (open triangles).

in Table 1. The results of $\bar{k}$ based on the self-consistent method and the Mori-Tanaka's theory are indicated by the red solid line (SC(ani)) and the blue solid one (MT(ani)), respectively. In the figure, the dashed line (SC(iso) and MT(iso)) shows the results when the thermal conductivity of the carbon filler is assumed to be isotropic, where the value of thermal conductivity in the radial direction is $1.6(W/(m \cdot K))$ same as that in the axial direction. From the figure, it can be seen that there is no significant difference in the results of $\bar{k}$ obtained by the self-consistent method and the Mori-Tanaka's theory when the carbon filler is anisotropic. The same is true for the results when the carbon filler is assumed to be isotropic. However, it can be seen that the tendency of $\bar{k}$ with respect to the aspect ratio of the filler ω_3 differs, depending on whether the carbon filler is treated as anisotropic or isotropic. When the carbon filler is treated as isotropic, as the value of ω_3 decreases and the shape of the filler approaches a flattened shape, $\bar{k}$ reaches a minimum at $\omega_3 = 1$ and then increases. This tendency is similar to Fig. 6. On the other hand, when the carbon filler is treated as anisotropic, $\bar{k}$

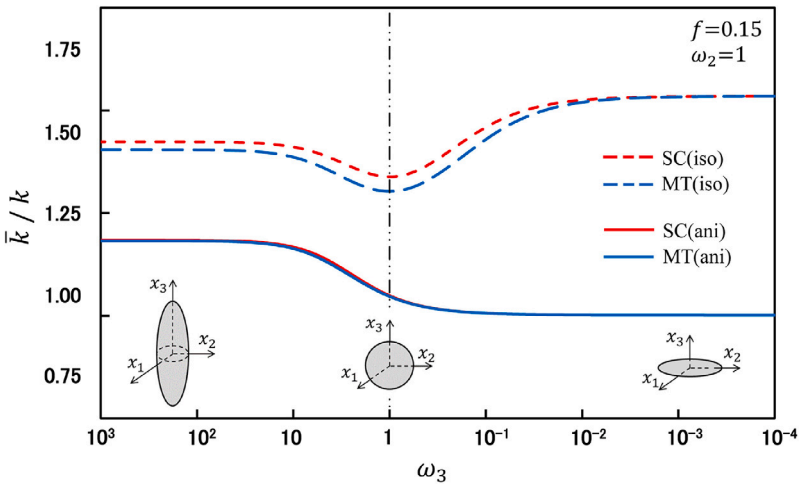

Fig. 10. Change in effective thermal conductivity $\overline{k}$ of anisotropic carbon (PAN-based)*3 filler / Polyethylene with the aspect ratio of filler. The solid red line and the solid blue one are the results of the self-consistent method and the Mori-Tanaka's theory respectively, in the case that the thermal conductivity of the filler in the axial direction (x_3 axis of the filler) is different from that in the radial one (x_1 or x_2 axis of the filler) as shown in Table 1. The dashed lines are the results in the case that the thermal conductivity of the filler in the radial direction is assumed to be equal to that of the axial direction.

decreases monotonically and takes the lowest value when the shape of the filler is flat. This is because the thermal conductivity of the filler in the radial direction is about 1/10 of that in the axial direction, as shown in Table 1. Therefore, the surface effect of the flattened filler mentioned in 4.2.1 tends to lower the $\overline{k}$. Comparing the result of the dashed line with that of the solid one, when the shape of the filler is flat, it is found that the result of the dashed line is about 1.5 times larger than that of the solid line, and the difference between two results is the largest at this shape of the filler. In the other hand, when the shape of the filler is long fibrous, the difference between two results is the smallest. In Figs. 6 and 7, the carbon filler was treated as isotropic, but it is assumed that the filler is actually anisotropic. As a result, there is no significant difference between the analytical results and the experimental ones, because the shape of the filler is treated as sphere or fibrous that the error is small regardless of whether the filler is treated as anisotropic or isotropic. Therefore, in the future, it will be necessary to compare the analytical results with the experimental ones when the shape of filler is flat. From the above, when the filler is oriented randomly in the material, it is very important to consider not only the shape of the filler but also its anisotropic properties in order to accurately evaluate the effective physical properties of the composite material. In addition, if the anisotropic properties of the filler are ignored and it is assumed to be isotropic, it is suggested that there is a possibility that a large error may occur when the shape of the filler is flat.

5. Conclusions

In this study, for a composite material containing anisotropic and ellipsoidal fillers oriented randomly in the matrix, the solution of the effective permittivity of the material can be derived explicitly by using the self-consistent method (SC) and the Mori-Tanaka's theory (MT). In addition, solutions of the effective permittivity both for composite materials containing many kinds of fillers with different shapes and physical properties and for polycrystalline materials can be also derived. In order to investigate the effect of the shape, the anisotropy, and the volume fraction of the filler on the effective physical properties of the material, we calculate the effective thermal conductivities of two types of composites and compare the obtained results with experimental ones.

As a result, for the isotropic carbon filler / polyethylene, it is found that the effective thermal conductivity of the material when the shape of the filler is flat is about 20% higher than that when the shape of the filler is fibrous, and the experimental results tend to be closer to the result of MT than that of SC as the aspect ratio decreases. Moreover, we analyze the case in which the anisotropic properties of the carbon filler are taken into account. As a result, when the shape of the filler is flat, the result when the filler is assumed to be isotropic is significantly different from that when the filler is assumed to be anisotropic. Therefore, when the filler is oriented randomly in the material, it is found that simultaneously considering not only the shape of the filler but also its anisotropic properties is important to accurately evaluate the effective physical properties of the composite material.

For two types of quartz particles (and voids) / polyethylene materials, the experimental result agrees better with the result of MT than that of SC, even if the volume fraction of the filler is more than 50%. In addition to this, since the tendency of the behavior of SC and MT with the volume fraction of the particle is the same as those of elastic moduli, the results of this analysis are considered to be reasonable to some extent. However, doubts remain about the differences between the results of SC and MT. MT uses the assumption that adding only one filler to the matrix does not affect the field in the material before this addition. When many kinds of fillers (including voids) exist in a material, it is obvious that the effect of adding one filler in the material on the interaction field differs depending on the shape and properties of the added filler. The solution based on MT obtained from this analysis does not consider this point. Thus, it is not clear at present whether the solution based on MT can correctly evaluate the interaction field

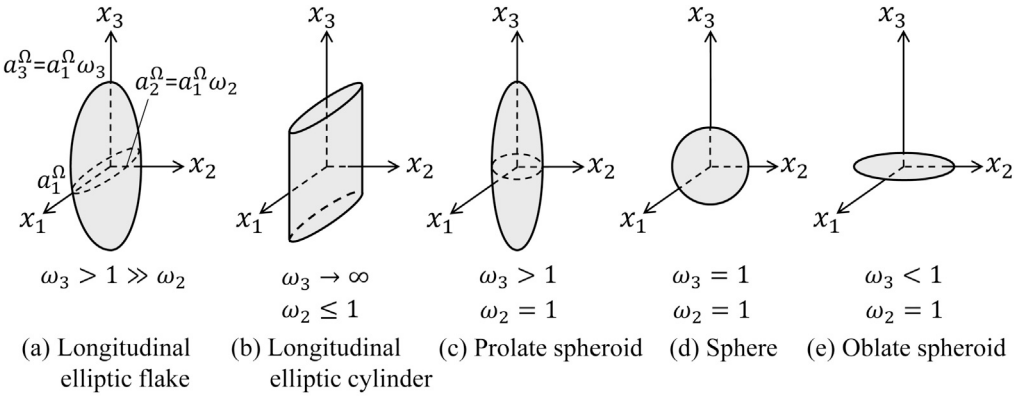

Fig. A. Various shapes of ellipsoidal filler.

inside the material containing many kinds of fillers. On the other hand, it is a well-known fact that the SC can accurately evaluate the interaction field for the high volume fraction of the filler.

From the above results, it is found that the analytical solutions of this study can generally explain the experimental results and can be applied to actual materials. However, it is considered that further investigation is required for the validity of the evaluation of interaction fields of many types of fillers, which is a subject for future study.

CRediT authorship contribution statement

Hiroyuki ONO: Conceived and designed the experiments; Performed the experiments; Analyzed and interpreted the data; Contributed reagents, materials, analysis tools or data; Wrote the paper.

Declaration of competing interest

The authors declare that they have no known competing financial interests or personal relationships that could have appeared to influence the work reported in this paper.

Data availability

Data included in article/supp. material/referenced in article.

Appendix A. Geometrical factor

Fig. A shows various shapes of ellipsoidal filler Ω. Fig. A(a) is called a longitudinal elliptic flake, which is thin in the x_2 direction and elongated in the x_3 direction. Fig. A(b) is called a longitudinal elliptic cylinder extended infinitely along the x_3 axis, and the cross-sectional shape in the $x_1 - x_2$ plane is an ellipse. Fig. A(c) is a prolate spheroid whose longitudinal direction is the x_3 axis, Fig. A(d) is a sphere and Fig. A(e) is an oblate spheroid and thin in the direction of the x_3 axis. The nonzero components of the geometrical factor H_i for these ellipsoidal shapes are expressed as

(a) Longitudinal elliptic flake ($\omega_3 > 1 \gg \omega_2$)

$$H_3^\Omega = \frac{\omega_2}{\omega_3^2-1}\left\{F(k)-E(k)\right\} \quad , \quad H_1^\Omega = -\frac{\omega_2}{\omega_3^2-1}\left\{F(k)-\omega_3^2 E(k)\right\} \quad , \quad H_2^\Omega = 1-\omega_2 E(k)\ , \tag{A.1a}$$

(b) Longitudinal elliptic cylinder ($\omega_3 \to \infty$, $\omega_2 \le 1$)

$$H_1^\Omega = \frac{\omega_2}{1+\omega_2} \quad , \quad H_2^\Omega = H_{23}^\Omega = \frac{1}{1+\omega_2}\ , \tag{A.1b}$$

(c) Prolate spheroid ($\omega_3 > 1$, $\omega_2 = 1$)

$$H_3^\Omega = 1-\frac{\omega_3}{(\omega_3^2-1)^{3/2}}\left\{\omega_3(\omega_3^2-1)^{1/2}-\cosh^{-1}\omega_3\right\} \quad , \quad H_1^\Omega = H_2^\Omega = \frac{1}{2}(1-H_3^\Omega)\ , \tag{A.1c}$$

(d) Sphere ($\omega_3 = \omega_2 = 1$)

$$H_3^\Omega = H_1^\Omega = H_2^\Omega = \frac{1}{3}\ , \tag{A.1d}$$

(e) oblate spheroid ($\omega_3 < 1$, $\omega_2 = 1$)

$$H_3^\Omega = 1-\frac{\omega_3}{(1-\omega_3^2)^{3/2}}\left\{\cos^{-1}\omega_3-\omega_3(1-\omega_3^2)^{1/2}\right\} \quad , \quad H_1^\Omega = H_2^\Omega = \frac{1}{2}(1-H_3^\Omega)\ , \tag{A.1e}$$

where ω_i in equations are aspect ratios of the filler, given by $\omega_2 = a_2^{\Omega}/a_1^{\Omega}$ and $\omega_3 = a_3^{\Omega}/a_1^{\Omega}$ as shown in Fig. A(a). $F(k)$ and $E(k)$ are complete elliptic integrals of the first and second kinds, and k is given by

$$k = \left(\frac{\omega_3^2 - 1}{\omega_3^2} \right)^{1/2} . \tag{A.2}$$

References

[1] X. Wang, M. Jiang, Z. Zhou, J. Gou, D. Hui, 3d printing of polymer matrix composites: a review and prospective, Composites, Part B, Eng. 110 (2017) 442–458, https://doi.org/10.1016/j.compositesb.2016.11.034.

[2] S.L. Zhai, P. Zhang, Y. Xian, J. Zeng, B. Shi, Review: Effective thermal conductivity of polymer composites: theoretical models and simulation models, Int. J. Heat Mass Transf. 117 (2018) 358–374, https://doi.org/10.1016/j.ijheatmasstransfer.2017.09.067.

[3] B. Sareni, L. Krähenbühl, A. Beroual, C. Brosseau, Effective dielectric constant of random composite materials, J. Appl. Phys. 81 (5) (1997) 2375–2383, https://doi.org/10.1063/1.364276.

[4] C. Wen-Zhong, T. Shan-Tung, T. Guo-Liang, Thermal conductivity of PTFE composites with three-dimensional randomly distributed fillers, J. Thermoplast. Compos. Mater. 18 (2005) 241–253, https://doi.org/10.1177/0892705705046900.

[5] T. Mori, K. Tanaka, Average stress in matrix and average elastic energy of materials with misfitting inclusions, Acta Metall. 21 (1973) 571–574, https://doi.org/10.1016/0001-6160(73)90064-3.

[6] B. Budiansky, On the elastic moduli of some heterogeneous materials, J. Mech. Phys. Solids 13 (1965) 223–227, https://doi.org/10.1016/0022-5096(65)90011-6.

[7] S. Nemat-Nasser, M. Hori, Micromechanics: Overall Properties of Heterogeneous Materials, North-Holland, 1993.

[8] Z. Hashin, S. Shtrikman, A variational approach the theory of the effective magnetic permeability of multiphase materials, J. Appl. Phys. 33 (1962) 3125–3131, https://doi.org/10.1063/1.1728579.

[9] Y. Benveniste, Effective thermal conductivity of composites with a thermal contact resistance between the constituents: nondilute case, J. Appl. Phys. 61 (1987) 2840–2843, https://doi.org/10.1063/1.337877.

[10] H. Hatta, M. Taya, Effective thermal conductivity of a misoriented short fiber composite, J. Appl. Phys. 58 (1985) 2478–2486, https://doi.org/10.1063/1.335924.

[11] T. Mura, Micromechanics of Defects in Solids, second revised edition, Kluwer Academic Publishers, 1987.

[12] H. Hatta, M. Taya, Equivalent inclusion method for steady state heat conduction in composites, Int. J. Eng. Sci. 24 (1986) 1159–1172, https://doi.org/10.1016/0020-7225(86)90011-X.

[13] S. Kanaun, V. Levin, Self-Consistent Methods for Composites Volume 1-Static Problems, Springer, 1986.

[14] H. Serkan, D. Kumlutas, I.H. Tavman, Effect of particle shape on thermal conductivity of copper reinforced polymer composites, J. Reinf. Plast. Compos. 26 (2007) 113–121, https://doi.org/10.1177/0731684407072522.

[15] S. Kemaloglu, G. Ozkoc, A. Aytac, Properties of thermally conductive micro and nano size boron nitride reinforced silicon rubber composites, Thermochim. Acta 499 (2010) 40–47, https://doi.org/10.1016/j.tca.2009.10.020.

[16] H.S. Göktürk, T.J. Fiske, D.M. Kalyon, Effects of particle shape and size distributions on the electrical and magnetic properties of nickel/polyethylene composites, J. Appl. Polym. Sci. 50 (1993) 1891–1901, https://doi.org/10.1002/app.1993.070501105.

[17] R. Wang, H. Zoberiri, H. Lin, W. Qu, X. Bai, C. Deng, X. Wang, Anisotropic thermal conductivities and structure in lignin-based microscale carbon fibers, Carbon 147 (2019) 58–69, https://doi.org/10.1016/j.carbon.2019.02.064.

[18] M.L. Minus, S. Kumar, The processing, properties, and structure of carbon fibers, JOM 57 (2005) 52–58, https://doi.org/10.1007/s11837-005-0217-8.

[19] M. Taya, Electric Composites, Cambridge University Press, 2005.

[20] S. Araki, H. Yamashita, H. Ono, Effect of change in shape of ellipsoidal reinforcement on macroscopic elastic moduli of a composite material, Trans. Jpn. Soc. Mech. Eng. 75 (760) (2009) 1702–1709, https://doi.org/10.1299/kikaia.75.1702.

[21] M. Toda, Classical Mechanics (An Introductory Course of Physics 1), Iwanami Shoten, 2002.

[22] Y. Agari, A. Ueda, M. Tanaka, S. Nagai, Thermal conductivity of a polymer filled with particles in the wide range from low to super-high volume content, J. Appl. Polym. Sci. 40 (1990) 929–941, https://doi.org/10.1002/app.1990.070400526.

[23] Y. Agari, A. Ueda, S. Nagai, Thermal conductivity of a polyethylene filled with disoriented short-cut carbon fibers, J. Appl. Polym. Sci. 43 (1991) 1117–1124, https://doi.org/10.1002/app.1991.070430612.

[24] X. Peng, N. Hu, H. Zheng, H. Fukunaga, Evaluation of mechanical properties of particulate composites with a combined self-consistent and Mori–Tanaka approach, Mech. Mater. 41 (2009) 1288–1297, https://doi.org/10.1016/j.mechmat.2009.07.006.